Geolocation Performance With Biased Range Measurements

Ning Liu, Zhengyuan Xu, *Senior Member, IEEE*, and Brian M. Sadler, *Fellow, IEEE*

***Abstract*—We study geolocation based on biased range estimates. Positive bias arises using time delay ranging methods in a multipath fading environment, when the line of sight direct path is severely attenuated. We model the range measurement as contaminated with Gaussian noise and an additive nonnegative bias term, and consider deterministic and random bias cases. We develop weighted least squares (WLS) and maximum likelihood (ML) geolocation estimators, and show that in general they yield biased geolocation estimates. A perturbation analysis technique is applied to find bias and mean square error (MSE) expressions for the WLS and MLE algorithms. MLE generally outperforms WLS, because MLE exploits knowledge of the range measurement bias distribution. The location error expressions are functions of the measurement bias and variance, as well as the network geometry. These results are useful to study achievable geolocation performance, and are applied to optimize sensor placement for improving the overall geolocation accuracy. We also develop the Cramér-Rao bound (CRB) on geolocation for our model. The CRB is a bound on unbiased estimation, whereas the geolocation algorithms may be biased, and we show how the estimators approach the CRB in certain cases. Numerical examples are presented to verify the analysis and study some cases of interest.**

***Index Terms*—Biased estimation, geolocation, multipath channel, nonline-of-sight (NLOS), range measurements, source localization, time delay.**

I. Introduction

WIRELESS geolocation employs distributed measurements to localize one or many nodes [2], [3]. The problem is important in sensor networking [4], emergency services [5], and other applications. A variety of measurement modalities may be used such as range, angle of arrival, time difference of arrival, Doppler shift, and received signal strength. These measurement types may be used separately or combined, and a joint in-network problem can be solved to simultaneously geolocate one or more nodes with pair-wise measurements among a mix of nodes some of which know their locations *a priori* [6]–[8]. As more nodes of known location are added, then more accurate joint solutions are possible. An alternative cooperative approach relies on a mobile platform to broadcast information that enables sensor nodes to geolocate themselves [9].

We consider geolocation of a node based on range estimates to sensors with known locations in a multipath fading propagation environment. The signal superposition at the receiver due to multipath induces strong fluctuation in received signal strength as the nodes or scatterers in the environment move. In addition, the line of sight (LOS) or direct path propagation may be severely attenuated due to obstructions, such that in many cases the LOS component of the signal is undetectable. Extensive microwave measurements have validated the Rayleigh/Rician model for LOS/NLOS propagation [10]–[12], and more recently indoor UWB measurements reveal that the LOS path is very often undetectable [13]–[15]. In this case the detectable signal arrives via nonline-of-sight (NLOS) propagation, and when used for ranging the additional propagation delay results in a positive bias on time delay and range estimation. Using these biased range measurements will then generally induce a biased location estimate.

We study the performance of geolocation estimators based on biased range estimates. We model the estimated range as having additive Gaussian measurement noise, as well as an additive nonnegative bias term, and we consider both deterministic and random modeling of the bias. Neglecting the bias leads to an additive white Gaussian noise (AWGN) model for the range measurements that is well studied in the context of geolocation (see references above), and leads to unbiased maximum-likelihood estimation (MLE) and corresponding Cramér-Rao bounds (CRBs). Deviating from the AWGN model however, can lead to biased geolocation estimates. For example, Patwari, *et al.*, considered geolocation based on inferring range from received signal strength, assuming a log-normal model and knowledge of the path loss parameter based on measurements [7]. They showed that in general for this case the MLE for geolocation is biased.

While the CRB is a bound on any unbiased estimator (subject to regularity conditions), geolocation estimators will generally exhibit bias when the range estimates are biased. Consequently, it is important to directly study the performance of geolocation algorithms, including both the estimation bias and mean-square error. Weiss and Picard considered a deterministic range bias model, where the bias is assumed to be constant for all sensors [16]. They developed a joint MLE for node location(s) and the bias parameter, and this estimator appears to achieve the CRB when the additive measurement bias becomes small,

Manuscript received August 20, 2011; revised December 16, 2011 and February 03, 2012; accepted February 04, 2012. Date of publication February 13, 2012; date of current version April 13, 2012. The associate editor coordinating the review of this manuscript and approving it for publication was Dr. Hing Cheung So. This work was supported in part by the Army Research Laboratory CTA on Communications and Networks by Grant DAAD19-01-2-0011 and by the National Nature Science Foundation of China by Grant 60928001. A preliminary version of this paper was presented at the 46th Annual Allerton Conference 2008, Urbana-Champaign, IL, September 2008 [1].

N. Liu was with the University of California, Riverside, CA. He is now with Broadcom Corporation, Irvine, CA 92617 USA (e-mail: ningliu@broadcom.com).

Z. Xu is with the Department of Electronic Engineering and Tsinghua National Laboratory of Information Science and Technology, Tsinghua University, Beijing 100084, P. R. China (e-mail: xuzy@tsinghua.edu.cn).

B. M. Sadler is with the Army Research Laboratory, Adelphi, MD 20783 USA (e-mail: brian.m.sadler6.civ@mail.mil).

Color versions of one or more of the figures in this paper are available online at http://ieeexplore.ieee.org.

Digital Object Identifier 10.1109/TSP.2012.2187645

and when the number of cooperating nodes in the network becomes large. Jourdan, *et al.*, considered a random measurement bias model and developed a CRB on location [17]. Employing a piece-wise constant bias model extracted from UWB measurements, and assuming the received signal SNR depends on range, they studied the geolocation CRB behavior with multiple beacons, but did not consider geolocation algorithms. Jourdan, *et al.*, showed that their CRB is reduced when additional range measurements are included, even if the measurement is biased. This is important because restricting attention only to unbiased estimators may lead to the unfounded conclusion that only direct path LOS measurements should be kept [18].

In this paper, starting with a deterministic measurement bias model, we study a weighted least squares (WLS) geolocation estimator. Then, considering a random measurement bias model, we derive a general expression for the geolocation MLE that accommodates any choice of bias distribution. To analyze the error performance of the WLS and MLE algorithms we use a small-error perturbation technique that provides expressions for the estimator bias and variance. This enables geolocation performance study as a function of the sensor placement geometry and the AWGN and range bias parameters, and reveals when bias dominates measurement noise or vice versa. We also compute the relevant CRBs, and show how the WLS and MLE algorithms revert to the CRB as the range bias becomes small.

We present our range measurement model in Section II, and consider the deterministic range bias case in Section III. Then in Section IV we consider a random bias with known distribution, and find a general expression for the geolocation MLE that can be evaluated for a given ranging bias distribution. The first-order perturbation error analysis is carried out for both of the above cases, and for random bias we study an exponential distribution in detail. In Section V we derive a general expression for the geolocation CRB with a random bias, which factors in a way that reveals the separate impact of sensor placement and measurement error distribution. In Section VI we present numerical examples to verify our analysis and study the impact of sensor placement and measurement error. The paper is concluded in Section VII.

II. Measurement Model

Consider a range-based 2-D localization problem employing K sensor nodes at known locations $\mathbf{p}_i = [x_i, y_i]^T, i = 1, \cdots, K$. The range from the signal source at $\mathbf{p}_{\rm s} = [x_s y_s]^T$ to the ith sensor at $\mathbf{p}_i$ is

$$d_i = \sqrt{(x_s - x_i)^2 + (y_s - y_i)^2}. \tag{1}$$

Let the angle between the source and the ith sensor with respect to the horizontal be θ_i, then

$$\cos\theta_i = \frac{x_s - x_i}{d_i}, \quad \sin\theta_i = \frac{y_s - y_i}{d_i}. \tag{2}$$

The range measurement at the ith sensor is modeled as

$$\begin{aligned} r_i &= d_i + v_i \\ &= d_i + b_i + n_i \end{aligned} \tag{3}$$

where $v_i = b_i + n_i$ is the total ranging error, composed of a nonnegative bias $b_i \geq 0$, and additive zero-mean Gaussian noise n_i with standard deviation σ_{n_i}.

This 2-D biased range measurement model can be easily extended to 3-D by defining $\mathbf{p}_i = [x_i, y_i, z_i]^T$ and $\mathbf{p}_{\rm s} = [x_s\ y_s\ z_s]^T$, with the obvious extension for range d_i so that (3) holds. Extending (2), the angles with respect to the x, y, z axes can be defined as

$$\cos\theta_{x_i} = \frac{x_s - x_i}{d_i}, \quad \cos\theta_{y_i} = \frac{y_s - y_i}{d_i}, \quad \cos\theta_{z_i} = \frac{z_s - z_i}{d_i}. \tag{4}$$

Note that only two of the three angles θ_{x_i}, θ_{y_i}, and θ_{z_i} are independent, and they are related by $\cos\theta_{x_i} = \sin\theta_{z_i}\cos\theta_i$ and $\cos\theta_{y_i} = \sin\theta_{z_i}\sin\theta_i$. In the following we focus on 2-D localization, pointing out the corresponding 3-D extensions as appropriate.

We consider estimation of $\mathbf{p}_{\rm s} = (x_s, y_s)$ based on the range measurements $\mathbf{r} = [r_1, \cdots, r_K]$. The positive bias models the impact of the additional time delay due to nonline of sight propagation, and we consider both deterministic and random models for the bias. For the random case, we employ a distribution on the time delay. Based on extensive measurements in microwave radio channels the most widely adopted time delay models include exponential, uniform, Maxwell, and Bernoulli distributions [10, pp. 340–341]. In this paper we primarily focus on the exponential time delay distribution, although the methodology is general and other distributions are readily adopted. We also assume that the sensors are sufficiently spread in the environment so that the bias measurements b_i are independent across sensors. The bias models are described next. Location estimators and error analysis for the deterministic case are developed in Section III, and for the random case in Section IV.

A. Exponential Distribution

With this model the bias follows an exponential distribution $\mathcal{E}\left(\frac{1}{\sigma_{b_i}}, b_i^0\right)$ with probability density function (pdf) given by

$$h_i(b_i) = \frac{1}{\sigma_{b_i}} \exp\left[-\frac{1}{\sigma_{b_i}}\left(b_i - b_i^0\right)\right], \quad b_i \geq b_i^0 \tag{5}$$

where b_i^0 is the origin (location parameter), and σ_{b_i} is both the mean and standard deviation of the variable $b_i - b_i^0$.

B. Uniform Distribution

Here, the bias b_i follows a uniform distribution in $[\beta_s, \beta_m]$ with pdf given by

$$h_i(b_i) = \begin{cases} \frac{1}{\beta_m - \beta_s} = \frac{1}{2\sqrt{3}\sigma_{b_i}} & \beta_s \leq b_i \leq \beta_m \\ 0 & \text{others} \end{cases} \tag{6}$$

where it is assumed that $\beta_s \geq 0$.

C. Maxwell Distribution

The Maxwell distribution has the following form

$$h_i(b_i) = \begin{cases} \frac{\sqrt{2/\pi}(3-8/\pi)^{3/2}}{\sigma_{b_i}^3} b_i^2 \exp\left[-\frac{(3-8/\pi)b_i^2}{2\sigma_{b_i}^2}\right] & b_i \geq 0 \\ 0 & b_i < 0 \end{cases} \tag{7}$$

with a distribution parameter σ_{b_i}.

With the above three random distributions, the time delay is modeled as more likely to be early (exponential), equally distributed over a known interval (uniform), or distributed around some most likely delay (Maxwell). The exponential model is the most widely adopted in the communications literature, and

has been experimentally validated in microwave channels. For example, the widely applied Jakes model for multipath mobile communications employs an exponential distribution for delay spread [11]. The uniform distribution can be employed if only an upper bound on delay is known. This can be refined if the environment can be specifically characterized, e.g., a piece-wise uniform distribution was applied in a cluttered indoor UWB scenario, modeling delay bias jumping from one maximum value to another depending on room size and obstacles [17]. Note the bias mean μ_{b_i} for each specific distribution model may vary even if it is assumed to have the same bias standard deviation σ_{b_i}.

III. Error Analysis and Performance Optimization for the Case of Deterministic Bias

In this section we assume the range bias errors b_i are deterministic and develop a weighted least squares (WLS) location estimator. The biased range measurements generally result in biased WLS location estimates. We study the WLS performance using a small-error perturbation technique, deriving mean square error (MSE) expressions that include both location estimate bias and variance. We then study the impact of sensor location, with an eye towards reducing the bias in the location estimate.

A. WLS Estimator

The WLS estimate of the source location is given by

$$\widehat{\mathbf{p}}_{\mathrm{s}}^{\mathrm{WLS}} = \min_{(x_s,y_s)} \sum_{i=1}^{K} (r_i - d_i)^2 w_i \tag{8}$$

where w_i is a weight that can be chosen as desired, for example, letting $w_i = \sigma_{n_i}^{-2}$. The solution to (8) occurs when the derivatives pass through zero. Differentiating (8) with respect to both x_s and y_s, and equating with zero we obtain [1]

$$\sum_{i=1}^{K} w_i (r_i - d_i) \cos\theta_i = 0 \tag{9}$$

$$\sum_{i=1}^{K} w_i (r_i - d_i) \sin\theta_i = 0. \tag{10}$$

These equations are highly nonlinear in x_s and y_s due to (1) and (2), but can readily be solved numerically.

B. First-Order Error Analysis of WLS Estimation

To study the estimation error of $\hat{\mathbf{p}}_{\mathrm{s}}^{\mathrm{WLS}}$, we next carry out a perturbation analysis around the optimal solution $\hat{\mathbf{p}}_{\mathrm{s}} = [\hat{x}_s, \hat{y}_s]^T$, e.g., see [19]. Let $\delta r_i = v_i$ denote a small measurement error that includes the measurement bias and noise. The error δr_i causes an estimation error $\delta x_s, \delta y_s$, and associated error δd_i in d_i. We assume the sensor postions x_i and y_i are known; sensor position errors can also be incorporated as additional perturbations.

Note that the perturbed quantities still satisfy (9) and (10). Under the small error assumption, perturbation analysis is equivalent to differentiation, i.e., replacing the total differential operator by the error operator δ at the true solution point. In order to relate δx_s and δy_s to δr_i, we first re-express δd_i. Using (1) and (2), and applying the total differential theorem, the first-order error terms are related by[1]

$$\delta d_i \approx \cos\theta_i \delta x_s + \sin\theta_i \delta y_s. \tag{11}$$

Next, we relate δx_s and δy_s to δr_i using (9) and (10), yielding two equations for δx_s and δy_s. Term-by-term differentiation of (9) and (10) yields

$$\sum_{i=1}^{K} w_i \left[(\delta r_i - \delta d_i) \cos\theta_i + (r_i - d_i)\delta(\cos\theta_i) \right] = 0 \tag{12}$$

$$\sum_{i=1}^{K} w_i \left[(\delta r_i - \delta d_i) \sin\theta_i + (r_i - d_i)\delta(\sin\theta_i) \right] = 0. \tag{13}$$

Here, r_i represents the measurement in the absence of error n_i, and δr_i represents the error v_i. Replacing r_i by d_i and δr_i by v_i, the above becomes

$$\sum_{i=1}^{K} w_i (v_i - \delta d_i) \cos\theta_i = 0 \tag{14}$$

$$\sum_{i=1}^{K} w_i (v_i - \delta d_i) \sin\theta_i = 0. \tag{15}$$

Substituting (11) into (14) and (15) and combining corresponding terms, we obtain a compact matrix equation for location estimation error vector $\delta\mathbf{p}$ given by

$$\mathbf{C}\delta\mathbf{p} \approx \mathbf{D}\mathbf{v} \tag{16}$$

where

$$\mathbf{C} = \begin{bmatrix} c_{11} & c_{12} \\ c_{21} & c_{22} \end{bmatrix}, \quad \delta\mathbf{p} = \begin{bmatrix} \delta x_s \\ \delta y_s \end{bmatrix}, \quad \mathbf{D} = \begin{bmatrix} \mathbf{d}_1^T \\ \mathbf{d}_2^T \end{bmatrix}$$
$$\mathbf{v} = [v_1 \ \cdots \ v_K]^T \tag{17}$$

with

$$c_{11} = \sum_{i=1}^{K} w_i \cos^2\theta_i, \quad c_{12} = c_{21} = \sum_{i=1}^{K} w_i \cos\theta_i \sin\theta_i$$
$$c_{22} = \sum_{i=1}^{K} w_i \sin^2\theta_i$$
$$\mathbf{d}_1 = [w_1 \cos\theta_1, \cdots, w_K \cos\theta_K]^T$$
$$\mathbf{d}_2 = [w_1 \sin\theta_1, \cdots, w_K \sin\theta_K]^T. \tag{18}$$

From (16), the first-order WLS estimation error vector is

$$\delta\mathbf{p} \approx \mathbf{C}^{-1}\mathbf{D}\mathbf{v}. \tag{19}$$

Eq. (19) is the desired relation between the location perturbation error $\delta\mathbf{p}$ and the system parameters. From this, the resulting MSE of the WLS location estimator is given by

$$\bar{\epsilon}_{\mathrm{WLS}}^2 = \mathbb{E}\left\{|\delta\mathbf{p}|^2\right\} \approx tr\{\mathbf{C}^{-1}\mathbf{D}\mathbf{\Phi}_v\mathbf{D}^T\mathbf{C}^{-1}\} \tag{20}$$

where $\mathbf{\Phi}_v$ is the correlation matrix of $\mathbf{v}$. Stacking the range bias from the different sensor measurements in the vector $\mathbf{b} =$

[1]This and related expressions in the following are equalities. We use $\approx$ to indicate that these expressions were derived under the small error assumption.

$[b_1, \cdots, b_K]^T$, then the correlation matrix is related to the bias and noise variance by

$$\mathbf{\Phi}_v = \mathbb{E}\{\mathbf{v}\mathbf{v}^T\} = \mathbf{R}_b + \text{diag}\left\{\sigma_{n_1}^2, \cdots, \sigma_{n_K}^2\right\} \tag{21}$$

where we define the deterministic correlation matrix $\mathbf{R}_b = \mathbf{b}\mathbf{b}^T$.

The resulting bias in the location estimate is given by

$$\beta_{\text{WLS}} = \mathbb{E}\{\delta\mathbf{p}\} \approx \mathbf{C}^{-1}\mathbf{D}\mathbf{b}. \tag{22}$$

Thus, the WLS estimate will be biased in general when $\mathbf{b} \neq \mathbf{0}$. However, note that the location bias can be small or zero while $\mathbf{b} \neq \mathbf{0}$, for example, when $\mathbf{C}^{-1}\mathbf{D}\mathbf{b} = \mathbf{0}$. The bias can be controlled to some extent with sensor placement. To examine this further, we next apply these expressions to study an example with a uniform circular sensor positioning.

Note the above approach can be extended to 3-D WLS estimation by applying the 3-D model in Section II to (8) and finding three equations similar to (9) and (10). The matrices $\mathbf{C}$ and $\mathbf{D}$ in the error analysis will also be expanded, involving d_i and the three angles $\theta_{x_i}, \theta_{y_i}, \theta_{z_i}$. When these are appropriately defined then the final error expressions in (19), (20), (21), and (22) still hold.

C. Example: Uniform Circular Sensor Placement

Consider an example where the sensors are uniformly and circularly placed around the source, so that $\theta_i = \frac{2\pi(i-1)}{K}$. This includes special cases of linear, triangular, and square sensor configurations, corresponding to $K = 2, 3, 4$, respectively. For simplicity in this example, we also assume a common measurement bias so that all elements in $\mathbf{b}$ are equal, i.e., $\mathbf{b} = b\mathbf{1}$ for $b \neq 0$, and we assume $w_i = w = \sigma_n^{-2}$ for all sensors. Under these assumptions, $\theta_i = \frac{2\pi(i-1)}{K}$ and the elements in $\mathbf{C}$ and vector $\mathbf{D}\mathbf{b}$ in (22) are given by

$$c_{11} = w\sum_{i=1}^{K}\cos^2\frac{2\pi(i-1)}{K} = \frac{1}{2}w[K + \sum_{i=1}^{K}\cos\frac{4\pi(i-1)}{K}] \tag{23}$$

$$c_{22} = w\sum_{i=1}^{K}\sin^2\frac{2\pi(i-1)}{K} = \frac{1}{2}w\left[K - \sum_{i=1}^{K}\cos\frac{4\pi(i-1)}{K}\right] \tag{24}$$

$$\begin{aligned} c_{12} = c_{21} &= w\sum_{i=1}^{K}\sin\frac{2\pi(i-1)}{K}\cos\frac{2\pi(i-1)}{K} \\ &= \frac{1}{2}w\sum_{i=1}^{K}\sin\frac{4\pi(i-1)}{K}, \end{aligned} \tag{25}$$

$$\mathbf{D}\mathbf{b} = wb\left[\sum_{i=1}^{K}\cos\frac{2\pi(i-1)}{K}, \sum_{i=1}^{K}\sin\frac{2\pi(i-1)}{K}\right]^T. \tag{26}$$

Using Euler's identities, $j = \sqrt{-1}$, and the geometric series expansion

$$\sum_{k=1}^{K} e^{j(k-1)x} = \frac{\sin\frac{Kx}{2}}{\sin\frac{x}{2}} e^{j\frac{K-1}{2}x} \tag{27}$$

we have

$$\sum_{k=1}^{K}\cos(k-1)x = \frac{\sin\frac{Kx}{2}\cos\frac{K-1}{2}x}{\sin\frac{x}{2}} \tag{28}$$

$$\sum_{k=1}^{K}\sin(k-1)x = \frac{\sin\frac{Kx}{2}\sin\frac{K-1}{2}x}{\sin\frac{x}{2}}. \tag{29}$$

Substituting these results into (23), (24), (25), and (26), we obtain

$$c_{11} = c_{22} = \frac{1}{2}wK, \quad c_{12} = c_{21} = 0, \quad \mathbf{D}\mathbf{b} = \mathbf{0}. \tag{30}$$

Therefore, $\mathbf{C} = \frac{wK}{2}\mathbf{I}$. Applying these results to (22) we find that $\mathbb{E}\{\delta\mathbf{p}\} = \mathbf{0}$. Thus, up to first-order error for this special geometry with common range measurement bias, the WLS location estimate is unbiased. It follows that small deviations in the sensor placement will result in relatively small bias in the location error, and indicates that spatially diverse sensor placement can reduce estimation bias.

The MSE (20) can also be simplified for this special case. With $\mathbf{D}\mathbf{b} = \mathbf{0}$ and $\text{diag}\{\sigma_1^2, \cdots, \sigma_K^2\} = \sigma^2\mathbf{I}$, it can be easily verified that $\mathbf{D}\mathbf{D}^T = w\mathbf{C}$. Then (20) becomes

$$\bar{\epsilon}_{\text{WLS}}^2 \approx \sigma_n^2 tr\{\mathbf{C}^{-1}\mathbf{D}\mathbf{D}^T\mathbf{C}^{-1}\} = \frac{4\sigma_n^2}{K}. \tag{31}$$

The expression is consistent with the CRB developed in [16, eq. (28)] for the case of a common deterministic bias for all sensors. It is interesting that without any knowledge of the common measurement bias, for this example, the WLS MSE approaches the CRB at high SNR (i.e., under the small error assumption).

D. Geolocation Performance Optimization

Our analytical results on the location estimation bias and MSE relate WLS performance to measurement bias, noise variance, sensor locations, and WLS weights. Here we consider adjusting the weights and sensor placement in order to minimize the localization error.

From (22), a general condition for WLS to produce an unbiased location estimate is $\mathbf{C}^{-1}\mathbf{D}\mathbf{b} = \mathbf{0}$. For this to be true, it is sufficient for $\mathbf{b}$ to be in the nullspace of $\mathbf{D}$, so that $\mathbf{D}\mathbf{b} = \mathbf{0}$, i.e., when

$$\sum_{i=1}^{K} w_i b_i \cos\theta_i = 0, \quad \sum_{i=1}^{K} w_i b_i \sin\theta_i = 0. \tag{32}$$

This sufficient condition suggests a possible method for sensor placement and weight selection that results in a small location estimation bias.

To gain some insight into bias reduction, let $b_i = b$ and $w_i = w$. The squared norm of $\mathbf{D}\mathbf{b}$ can now be expressed as

$$\begin{aligned} |\mathbf{D}\mathbf{b}|^2 &= b^2w^2\left[\left(\sum_{i=1}^{K}\cos\theta_i\right)^2 + \left(\sum_{i=1}^{K}\sin\theta_i\right)^2\right] \\ &= b^2w^2\left[K + \sum_{i_1\neq i_2=1}^{K}\cos\left(\theta_{i_1} - \theta_{i_2}\right)\right]. \end{aligned} \tag{33}$$

This quantity depends on the measurement bias b and all possible sensor placement angle differences. For example, consider a placement where all the sensors are located in a single cluster around angle zero with respect to the source, but not exactly at the same position so that identifiability holds and localization is possible. Then, $|\mathbf{D}\mathbf{b}|^2$ is very close to its maximum value

of $K^2b^2w^2$ since all θ_i are almost equal. This worst case leads to a large estimation bias and consequently an increased MSE. Now suppose half of the (presumed even number of) sensors are clustered at angle zero, and the other half at angle 180 degrees. Then, $|\mathbf{Db}|^2$ reaches its minimum value of zero, and $\hat{\mathbf{p}}_{\rm s}^{\rm WLS}$ is unbiased. This is similar to the circular array case discussed in Section III-C. For arbitrary sensor configurations, $|\mathbf{Db}|^2$ takes a value between zero and its maximum. For example, if half the sensors are at angle zero and half at 90 degrees, then $|\mathbf{Db}|^2$ takes the medium value $\frac{K^2b^2w^2}{2}$. These examples indicate that sensor location angle diversity helps to reduce the impact of measurement bias.

It is clear that diversifying the sensor placement can reduce the WLS bias. In addition, the WLS weights can be employed to reduce the localization error. From (32), the weight for a particular sensor should be made smaller when the bias is larger. Alternatively, a bias-variance tradeoff could be attained by minimizing the MSE in (20) with respect to both sensor locations and weights.[2] The WLS algorithm brings flexibility, enabling exploitation of prior knowledge when it is available to tune the weights.

IV. Maximum-Likelihood Estimation and Its Error Analysis for the Case of Random Bias

In this section we assume the range bias errors b_i are random, and find the MLE for location. Generally, the biased range estimates cause the MLE of the location to be biased. To analyze the MLE performance, we employ the small-error perturbation analysis approach to find its MSE, similar to the deterministic case in the previous section. Later we develop the CRB for unbiased location estimators, and in Section VI we consider some cases when unbiased estimation is possible, enabling comparison with the CRB.

With random range bias in the measurement model (3), the measurement error v_i is the sum of independent random bias b_i and Gaussian noise n_i, so the distribution of v_i is the convolution of the two pdfs. We set up this model and find the general form of the MLE optimization problem. We then apply the perturbation technique to find an analytical expression for the MSE of the MLE. From this general result, we study the case of exponentially distributed bias in detail. In Appendix II we establish an equivalence of this random model with the deterministic bias case under the limit of the bias standard deviation $\sigma_{b_i} \to 0$.

A. General Location Error Analysis Procedure for a Random Bias Model

With the random bias assumption and sensor measurement model (3), the distribution $f_i(v_i)$ of v_i is the convolution of the bias pdf $h_i(b_i)$ and the noise pdf $g_i(n_i)$, given by

$$f_i(v_i) = \int_{-\infty}^{\infty} h_i(x) g_i(v_i - x) dx \tag{34}$$

[2]A related approach models the measurement noise variance to depend deterministically on range, so closer sensors have higher SNR, and this can also be treated in the WLS setting. However, in a NLOS fading environment the SNR has rapid spatial fluctuation, and so inferring range from observed SNR can be highly inaccurate.

where the Gaussian distribution of n_i is

$$g_i(n_i) = \frac{1}{\sqrt{2\pi}\sigma_{n_i}} e^{-\frac{n_i^2}{2\sigma_{n_i}^2}}. \tag{35}$$

With our assumption that all b_i and n_i are independent, the joint pdf of all range measurements $r_i = d_i + b_i + n_i$ is simply the product of the individual pdfs. Thus, the ML estimator can be obtained from the log-likelihood function given by

$$\begin{aligned}\widehat{\mathbf{p}}_{\rm s}^{\rm ML} &= \max_{(x_s, y_s)} \mathcal{L} = \ln f(\mathbf{r}; \mathbf{p}_{\rm s}) \\ &= \ln \prod_{i=1}^{K} f_i(r_i - d_i) = \sum_{i=1}^{K} \ln f_i(r_i - d_i). \end{aligned} \tag{36}$$

The MLE will be a solution of the two equations obtained by setting the partial derivatives of $\mathcal{L}$ with respect to x_s and y_s equal to zero, given by

$$\sum_{i=1}^{K} \frac{f_i'(r_i - d_i)}{f_i(r_i - d_i)} \cos\theta_i = 0 \tag{37}$$

$$\sum_{i=1}^{K} \frac{f_i'(r_i - d_i)}{f_i(r_i - d_i)} \sin\theta_i = 0. \tag{38}$$

Here, $f_i'(r_i - d_i)$ is the derivative with respect to d_i, which can be found from the derivative of $f_i(v_i)$ with respect to v_i since $f_i'(r_i - d_i) = -f_i'(v_i)$. We emphasize that these equations are general for the range-based localization model. For a specific bias pdf model $h_i(b_i)$ we substitute $f_i'(v_i)$ or $f_i'(r_i - d_i)$ into (37) and (38), and the MLE of x_s and y_s will be a solution. Next we analyze the MLE using the first-order perturbation approach as we did in Section III-B for the WLS estimator.

B. Error Analysis Under the Exponential Bias Distribution Model

We expand (37) and (38) around $r_i = d_i + b_i^0$ to obtain two equations, which build the connection of δx_s and δy_s with the first-order perturbation in the range measurement $\delta r_i = v_i - b_i^0 = b_i - b_i^0 + n_i$. As we did in Section III-B, these equations can be written in matrix form and solved for location error vector $\delta\mathbf{p}$. The bias and variance of $\hat{\mathbf{p}}_{\rm s}^{\rm ML}$ then follow easily. The measurement error distributions for the uniform and Maxwell bias distributions are given in Appendix I.

1) Distribution of Measurement Error: Assume the bias b_i at the ith sensor follows an exponential distribution $\mathcal{E}\left(\frac{1}{\sigma_{b_i}}, b_i^0\right)$ given by (5). From (34), the pdf of v_i is

$$\begin{aligned} f_i(v_i) &= \int_{b_i^0}^{\infty} h_i(x) g_i(v_i - x) dx \\ &= \frac{1}{\sqrt{2\pi}\sigma_{n_i}\sigma_{b_i}} \int_{b_i^0}^{\infty} \exp\left(-\frac{x - b_i^0}{\sigma_{b_i}}\right) \\ &\qquad \times \exp\left[-\frac{(v_i - x)^2}{2\sigma_{n_i}^2}\right] dx. \end{aligned} \tag{39}$$

This can be simplified to obtain

$$f_i(v_i) = \frac{1}{\sqrt{2\pi}\sigma_{n_i}\sigma_{b_i}} \exp\left(\frac{b_i^0 - v_i}{\sigma_{b_i}} + \frac{\sigma_{n_i}^2}{2\sigma_{b_i}^2}\right) \times \int_{b_i^0}^{\infty} \exp\left[-\frac{\left(x - v_i + \sigma_{n_i}^2/\sigma_{b_i}\right)^2}{2\sigma_{n_i}^2}\right] dx = \frac{1}{\sigma_{b_i}} \exp\left(\frac{b_i^0 - v_i}{\sigma_{b_i}} + \frac{\sigma_{n_i}^2}{2\sigma_{b_i}^2}\right) Q\left(\frac{b_i^0 - v_i + \sigma_{n_i}^2/\sigma_{b_i}}{\sigma_{n_i}}\right) \quad (40)$$

where $Q(\cdot)$ is the Q-function. Note that at $v_i = b_i^0$ we obtain

$$f_i\left(b_i^0\right) = \frac{1}{\sigma_{b_i}} e^{\frac{\sigma_{n_i}^2}{2\sigma_{b_i}^2}} Q\left(\frac{\sigma_{n_i}}{\sigma_{b_i}}\right). \quad (41)$$

2) ML Estimator: To evaluate (37) and (38), we find the derivative of $f_i(v_i)$ in (40) with respect to v_i. Differentiation under the integral sign for function $F(x)$

$$F(x) = \int_{a(x)}^{b(x)} f(x,t)dt$$

is given by

$$\frac{dF(x)}{dx} = f\left(x, b(x)\right)\frac{db(x)}{dx} - f\left(x, a(x)\right)\frac{da(x)}{dx} + \int_{a(x)}^{b(x)} \frac{\partial}{\partial x} f(x,t)dt. \quad (42)$$

Using the definition of the Q-function we have

$$\frac{d}{dv_i} Q\left(\frac{b_i^0 - v_i + \sigma_{n_i}^2/\sigma_{b_i}}{\sigma_{n_i}}\right) = \frac{1}{\sqrt{2\pi}\sigma_{n_i}} \exp\left[-\frac{\left(b_i^0 - v_i + \sigma_{n_i}^2/\sigma_{b_i}\right)^2}{2\sigma_{n_i}^2}\right]. \quad (43)$$

Applying (43) to (40) we find

$$f_i'(v_i) = -\frac{1}{\sigma_{b_i}} f_i(v_i) + \frac{1}{\sigma_{b_i}\sqrt{2\pi}\sigma_{n_i}} \exp\left[-\frac{\left(v_i - b_i^0\right)^2}{2\sigma_{n_i}^2}\right] = \frac{1}{\sigma_{b_i}}\left[g_i\left(v_i - b_i^0\right) - f_i(v_i)\right]. \quad (44)$$

Using (44) in (37) and (38), the constraint equations for the ML estimator become

$$\sum_{i=1}^{K} \frac{1}{\sigma_{b_i}} \left[\frac{g_i\left(r_i - d_i - b_i^0\right)}{f_i(r_i - d_i)} - 1\right] \cos\theta_i = 0 \quad (45)$$

$$\sum_{i=1}^{K} \frac{1}{\sigma_{b_i}} \left[\frac{g_i\left(r_i - d_i - b_i^0\right)}{f_i(r_i - d_i)} - 1\right] \sin\theta_i = 0. \quad (46)$$

Substituting (35) and (40), and recalling (1) and (2), we obtain the desired nonlinear equations expressed in terms of x_s and y_s. Next we carry out the perturbation analysis to analyze the MLE performance.

3) Error Analysis of the Geolocation MLE: The perturbed estimates still satisfy (45) and (46). We expand them around $r_i = d_i + b_i^0$ to obtain two equations for δx_s and δy_s with the perturbation in the range measurement $\delta r_i = v_i - b_i^0 = b_i - b_i^0 + n_i$ as input. For notational simplicity, we focus on the ith term in the summation, and also temporarily suppress the multiplicative constant $\frac{1}{\sigma_{b_i}}$. Later on we will put both the summation and this constant back. Applying the differential theorem to the left hand sides of (45) and (46), we obtain

$$\delta\left[\frac{g_i\left(r_i - d_i - b_i^0\right)}{f_i(r_i - d_i)}\right]\cos\theta_i + \left[\frac{g_i\left(r_i - d_i - b_i^0\right)}{f_i(r_i - d_i)} - 1\right]\delta(\cos\theta_i) \quad (47)$$

$$\delta\left[\frac{g_i\left(r_i - d_i - b_i^0\right)}{f_i(r_i - d_i)}\right]\sin\theta_i + \left[\frac{g_i\left(r_i - d_i - b_i^0\right)}{f_i(r_i - d_i)} - 1\right]\delta(\sin\theta_i). \quad (48)$$

Under the small perturbation assumption we have

$$\delta g_i\left(r_i - d_i - b_i^0\right) \approx g_i'\left(r_i - d_i - b_i^0\right)\left(\delta r_i - \delta d_i\right) \quad (49)$$

$$\delta f_i(r_i - d_i) \approx f_i'(r_i - d_i)(\delta r_i - \delta d_i) \quad (50)$$

and $r_i = d_i + b_i^0$. Now, the first error term in (47) and (48) is given by

$$\delta\left[\frac{g_i\left(r_i - d_i - b_i^0\right)}{f_i(r_i - d_i)}\right] \approx \frac{g_i'(0) f_i\left(b_i^0\right) - g_i(0) f_i'\left(b_i^0\right)}{f_i^2\left(b_i^0\right)}(\delta r_i - \delta d_i). \quad (51)$$

According to (35), $g_i'(0) = 0$. Also together with (35) and (44), we obtain

$$f_i'\left(b_i^0\right) = \frac{1}{\sigma_{b_i}}\left[g_i(0) - f_i\left(b_i^0\right)\right], \quad g_i(0) = \frac{1}{\sqrt{2\pi}\sigma_{n_i}} \quad (52)$$

where $f_i(b_i^0)$ is given by (41). Substituting (52) and (11) into (51), we obtain

$$\delta\left[\frac{g_i\left(r_i - d_i - b_i^0\right)}{f_i(r_i - d_i)}\right] \approx \frac{g_i(0) f_i'\left(b_i^0\right)}{f_i^2\left(b_i^0\right)} \times (\cos\theta_i \delta x_s + \sin\theta_i \delta y_s - \delta r_i). \quad (53)$$

The second error terms in (47) and (48) are now

$$\delta(\cos\theta_i) \approx \frac{\sin\theta_i}{d_i}(\sin\theta_i \delta x_s - \cos\theta_i \delta y_s) \quad (54)$$

$$\delta(\sin\theta_i) \approx -\frac{\cos\theta_i}{d_i}(\sin\theta_i \delta x_s - \cos\theta_i \delta y_s). \quad (55)$$

Substituting (52), (53), (54) and (55) into (47) and (48), and including the summation and the multiplicative constant $\frac{1}{\sigma_{b_i}}$, we obtain

$$u_{11}\delta x_s + u_{12}\delta y_s \approx \mathbf{t}_1^T \delta\mathbf{r} \quad (56)$$

$$u_{21}\delta x_s + u_{22}\delta y_s \approx \mathbf{t}_2^T \delta\mathbf{r} \quad (57)$$

with

$$u_{11} = \sum_{i=1}^{K} \frac{\left[g_i(0) - f_i\left(b_i^0\right)\right]}{\sigma_{b_i} d_i f_i^2\left(b_i^0\right)} \times \left[\frac{d_i g_i(0)\cos^2\theta_i}{\sigma_{b_i}} + f_i\left(b_i^0\right)\sin^2\theta_i\right] \tag{58}$$

$$u_{12} = u_{21} = \sum_{i=1}^{K} \frac{\left[g_i(0) - f_i\left(b_i^0\right)\right]\sin 2\theta_i}{2\sigma_{b_i} d_i f_i^2\left(b_i^0\right)} \times \left[\frac{d_i g_i(0)}{\sigma_{b_i}} - f_i\left(b_i^0\right)\right] \tag{59}$$

$$u_{22} = \sum_{i=1}^{K} \frac{\left[g_i(0) - f_i\left(b_i^0\right)\right]}{\sigma_{b_i} d_i f_i^2\left(b_i^0\right)} \times \left[\frac{d_i g_i(0)\sin^2\theta_i}{\sigma_{b_i}} + f_i\left(b_i^0\right)\cos^2\theta_i\right] \tag{60}$$

$$\mathbf{t}_1 = [t_{1,1}, \cdots, t_{1,K}]^T, \quad \mathbf{t}_2 = [t_{2,1}, \cdots, t_{2,K}]^T \tag{61}$$

$$t_{1,i} = \frac{g_i(0)\left[g_i(0) - f_i\left(b_i^0\right)\right]\cos\theta_i}{\sigma_{b_i}^2 f_i^2\left(b_i^0\right)}$$

$$t_{2,i} = \frac{g_i(0)\left[g_i(0) - f_i\left(b_i^0\right)\right]\sin\theta_i}{\sigma_{b_i}^2 f_i^2\left(b_i^0\right)}. \tag{62}$$

These equations can be compactly written in the matrix form

$$\mathbf{U}\delta\mathbf{p} \approx \mathbf{T}\delta\mathbf{r}. \tag{63}$$

So, from (63), the first order estimation error vector for source location in this case is

$$\delta\mathbf{p} \approx \mathbf{U}^{-1}\mathbf{T}\delta\mathbf{r}. \tag{64}$$

We obtain the MLE bias and MSE as follows. Since

$$\mathbb{E}\{\delta r_i\} = \sigma_{b_i}, \quad \mathbb{E}\left\{(\delta r_i)^2\right\} = 2\sigma_{b_i}^2 + \sigma_{n_i}^2$$

and the mean and correlation of the vector $\delta\mathbf{r}$ are given by

$$\boldsymbol{\mu}_b = \mathbb{E}\{\delta\mathbf{r}\} = [\sigma_{b_1}, \cdots, \sigma_{b_K}]^T$$

$$\boldsymbol{\Psi} = \mathbb{E}\{\delta\mathbf{r}\delta\mathbf{r}^T\} = \boldsymbol{\mu}_b\boldsymbol{\mu}_b^T + \operatorname{diag}\left\{\left(\sigma_{b_1}^2 + \sigma_{n_1}^2\right), \cdots, \left(\sigma_{b_K}^2 + \sigma_{n_K}^2\right)\right\}$$

then the bias and MSE of the location estimate are given by

$$\beta_{\mathrm{ML}} = \mathbb{E}\{\delta\mathbf{p}\} \approx \mathbf{U}^{-1}\mathbf{T}\boldsymbol{\mu}_b \tag{65}$$

$$\epsilon_{\mathrm{ML}}^2 = \mathbb{E}\{\delta\mathbf{p}^T\delta\mathbf{p}\} \approx tr\{\mathbf{U}^{-1}\mathbf{T}\boldsymbol{\Psi}\mathbf{T}^T\mathbf{U}^{-1}\}. \tag{66}$$

The extension to 3-D proceeds by applying the 3-D measurement model to the log-likelihood function (36). Differentiating results in three MLE constraint equations in $d_i, \theta_{x_i}, \theta_{y_i}$ and θ_{z_i}, similar to (37) and (38). The error analysis will be based on the perturbation of the three independent variables, leading to more complicated expressions for the coefficients matrices $\mathbf{U}$ and $\mathbf{T}$. The resulting error expressions will have the same form as (64), (65) and (66). The noise and bias distributions $g_i(n_i)$ and $f_i(v_i)$ in (35) and (40) hold without change.

The bias and MSE of $\hat{\mathbf{p}}_{\mathrm{s}}^{\mathrm{ML}}$ are functions of the number and location of the sensors, the bias distribution parameters, and the additive noise variance. One extreme case is when $\sigma_{b_i} \to 0$, the random bias diminishes. Then the exponential bias model converges to the deterministic bias case, and the error analyses are equivalent. We show the detailed analysis for this limiting case in Appendix II.

V. CRBs

In this section, we derive the localization CRB for the noisy range measurement models presented. Although the CRB is only valid for unbiased position estimators, the bound will be useful for comparison in the examples presented in Section VI. Under the independent measurement assumption, the joint distribution of the range measurement vector $\mathbf{r} = [r_1, r_2, \cdots, r_K]$ is the product

$$f(\mathbf{r}; \mathbf{p}_{\mathrm{s}}) = \prod_{i=1}^{K} f_i(r_i; \mathbf{p}_{\mathrm{s}}). \tag{67}$$

The Fisher information matrix (FIM) for estimation of $\mathbf{p}_{\mathrm{s}}$ is given by

$$\mathbf{J} = \mathbb{E}_{\mathbf{r}}\left\{\left[\nabla_{\mathbf{p}_{\mathrm{s}}} \ln\left(f(\mathbf{r}; \mathbf{p}_{\mathrm{s}})\right)\right]\left[\nabla_{\mathbf{p}_{\mathrm{s}}} \ln\left(f(\mathbf{r}; \mathbf{p}_{\mathrm{s}})\right)\right]^T\right\} = \sum_{i=1}^{K} \rho(\nu_i) \begin{bmatrix} \cos^2\theta_i & \cos\theta_i \sin\theta_i \\ \sin\theta_i \cos\theta_i & \sin^2\theta_i \end{bmatrix} \tag{68}$$

where

$$\nu_i = v_i - \mu_{b_i} = r_i - d_i - \mu_{b_i}$$

$$\rho(\nu_i) = \int_{-\infty}^{\infty} \frac{1}{f_i(r_i; \mathbf{p}_{\mathrm{s}})} \left(\frac{\partial f_i(r_i; \mathbf{p}_{\mathrm{s}})}{\partial d_i}\right)^2 d\nu_i. \tag{69}$$

The CRB is obtained from the diagonal elements of the inverse of the FIM, given by

$$\mathbb{E}_{\mathbf{r}}\left\{(\mathbf{p}_{\mathrm{s}} - \widehat{\mathbf{p}}_{\mathrm{s}})(\mathbf{p}_{\mathrm{s}} - \widehat{\mathbf{p}}_{\mathrm{s}})^T\right\} \geq \mathbf{J}^{-1}. \tag{70}$$

Extending to 3-D localization, the FIM is the same as (68) except that the angle matrix will involve any two independent variables from θ_{x_i}, θ_{y_i}, and θ_{z_i}. The dimensions of both the angle matrix and the FIM are extended to 3×3 corresponding to the x, y, z coordinates.

The FIM has an interesting interpretation, since in (68) $\mathbf{J}$ factors into the product of $\rho(\nu_i)$ that depends on the composite measurement error pdf, and a matrix that depends only on the angles θ_i of the sensors. This factorization, into a term that depends on the pdf and a term that doesn't, is expected, since the FIM for an arbitrary parametric signal model in additive i.i.d. non-Gaussian or Gaussian noise follows this form [20]. A similar FIM on localization is found in [17], where the bias distribution is modeled as piecewise uniformly distributed and the AWGN variance is modeled to be dependent on the range.

To characterize the position error with a scalar quantity it is convenient to use the root-mean-squared error (RMSE), given by

$$\mathrm{RMSE} \triangleq \sqrt{\mathbb{E}_{\mathbf{r}}\left\{(x_s - \widehat{x}_s)^2 + (y_s - \widehat{y}_s)^2\right\}} \geq \sqrt{tr\{\mathbf{J}^{-1}\}} \tag{71}$$

where tr denotes the trace of a square matrix.

The FIM and resulting CRB are easily evaluated for a given measurement error distribution $f_i(r_i;\mathbf{p}_s) = f_{v_i}(v_i)$. The integral for $\rho(\nu_i)$ in (69) has a closed form for some pdf cases of interest such as Gaussian, e.g., see [20], otherwise it can be readily evaluated numerically. In the remainder of this section we provide details for the three random bias models of interest. For convenience, we denote $f_i(r_i) = f_i(r_i;\mathbf{p}_s)$ from now on.

A. Exponential Bias Model

When the bias b_i follows the exponential distribution in (5), then the pdf of r_i is given by

$$f_i(r_i) = \frac{1}{\sigma_{b_i}} \exp\left(\frac{b_i^0 - r_i + d_i}{\sigma_{b_i}} + \frac{\sigma_{n_i}^2}{2\sigma_{b_i}^2}\right) \times Q\left(\frac{b_i^0 - r_i + d_i + \sigma_{n_i}^2/\sigma_{b_i}}{\sigma_{n_i}}\right). \quad (72)$$

The derivative of (72) with respect to d_i is

$$\frac{\partial f_i(r_i)}{\partial d_i} = \frac{1}{\sigma_{b_i}}\left[f_i(r_i) - g_i\left(r_i - d_i - b_i^0\right)\right] \quad (73)$$

where $g_i(r_i - d_i - b_i^0)$ is the Gaussian noise pdf in (35). Substituting (73) into (69) we obtain

$$\rho(\nu_i) = \int_{-\infty}^{\infty} \frac{\left[f_i(r_i) - g_i\left(r_i - d_i - b_i^0\right)\right]^2}{\sigma_{b_i}^2 f_i(r_i)} d\nu_i. \quad (74)$$

The CRB is then obtained by substituting $\rho(\nu_i)$ into (68) and using (70).

We remark that this CRB does not exist if all $\sigma_{n_i} \to 0$, i.e., when the Gaussian noise diminishes while the measurement bias distribution remains fixed. It naturally follows that from (40), and due to $v_i \geq b_i^0$ and $Q(-\infty) = 1$, that now $f_i(v_i)$ reduces to an exponential pdf form given by

$$f_i(v_i) = \frac{1}{\sigma_{b_i}} \exp\left[-\frac{1}{\sigma_{b_i}}\left(v_i - b_i^0\right)\right], \quad v_i \geq b_i^0. \quad (75)$$

This distribution does not satisfy the regularity condition, thus there is no CRB for this limiting case. Furthermore, the ML estimator needs to satisfy (36), which reduces to

$$\max_{(x_s,y_s)} \mathcal{L} = \sum_{i=1}^{K}\left[-\ln\sigma_{b_i} - \frac{1}{\sigma_{b_i}}\left(r_i - d_i - b_i^0\right)\right]. \quad (76)$$

Its partial derivatives with respective to x_s and y_s become

$$\frac{\partial \mathcal{L}}{\partial x_s} = \sum_{i=1}^{K} \frac{\cos\theta_i}{\sigma_{b_i}}, \quad \frac{\partial \mathcal{L}}{\partial y_s} = \sum_{i=1}^{K} \frac{\sin\theta_i}{\sigma_{b_i}}.$$

The partial derivatives are independent of d_i and (x_s, y_s) and the objective function $\mathcal{L}$ increases without bound in the unknowns (x_s, y_s), so in this case the MLE does not exist.

B. Uniform Bias Model

When the bias b_i follows the uniform distribution in $[\beta_s, \beta_m]$, the pdf of r_i is given by

$$f_i(r_i) = \frac{1}{\beta_m - \beta_s}\left[Q\left(\frac{r_i - d_i - \beta_m}{\sigma_n}\right) - Q\left(\frac{r_i - d_i - \beta_s}{\sigma_n}\right)\right] \quad (77)$$

which is a special case of the piecewise uniform model in [17]. The derivative is

$$\frac{\partial f_i(r_i)}{\partial d_i} = \frac{e^{-(r_i - d_i - \beta_m)^2/2\sigma_n^2} - e^{-(r_i - d_i - \beta_s)^2/2\sigma_n^2}}{\sqrt{2\pi}\sigma_n(\beta_m - \beta_s)} \quad (78)$$

and $\rho(\nu_i)$ can be obtained using (69).

C. Maxwell Bias Model

From (81), the pdf of r_i is

$$f_i(r_i) = \frac{(3 - 8/\pi)^{3/2}}{\pi\sigma_{b_i}^3\sigma_n} \times \int_0^{\infty} x^2 \exp\left[-\frac{(3 - 8/\pi)x^2}{2\sigma_{b_i}^2} - \frac{(r_i - d_i - x)^2}{2\sigma_n^2}\right] dx. \quad (79)$$

The derivative of $f_i(r_i)$ is

$$\frac{\partial f_i(r_i)}{\partial d_i} = \frac{(3 - 8/\pi)^{3/2}}{\pi\sigma_{b_i}^3\sigma_n^3} \int_0^{\infty} x^2(r_i - d_i - x) \times \exp\left[-\frac{(3 - 8/\pi)x^2}{2\sigma_{b_i}^2} - \frac{(r_i - d_i - x)^2}{2\sigma_n^2}\right] dx \quad (80)$$

and $\rho(\nu_i)$ can be obtained numerically.

VI. Numerical Results

In this section, we present numerical results for the WLS and MLE algorithms, their small error performance analysis, and the CRB. We generally assume the exponential random bias model; a later example also compares with a uniform bias distribution. To plot source location estimation performance, we adopt the root mean-square-error (RMSE) and estimation bias, e.g., see [19]

$$\text{RMSE} = \sqrt{E\left\{(\delta x_s)^2\right\} + E\left\{(\delta y_s)^2\right\}}$$
$$\text{Bias} = \sqrt{\left(E\{\delta x_s\}\right)^2 + \left(E\{\delta y_s\}\right)^2}.$$

We examine the effects of measurement bias pdf parameters $\boldsymbol{\mu}_b$ and $\boldsymbol{\sigma}_b$ and AWGN variance $\boldsymbol{\sigma}_n$, and the sensor geometry. WLS and MLE simulations are based on 50 000 Monte Carlo realizations, where the above expectations in the RMSE and bias are calculated using sample averages.

We begin with $K = 10$ sensors at fixed positions, and consider uniform and nonuniform spacing on a circle with normalized radius of one distance unit (DU), centered at the (unknown) source location. The exponentially distributed bias and the Gaussian noise at each sensor are assumed i.i.d. with $\sigma_{b_i} = \sigma_b$ and $\sigma_{n_i} = \sigma_n$, unless stated otherwise. Note that the errors

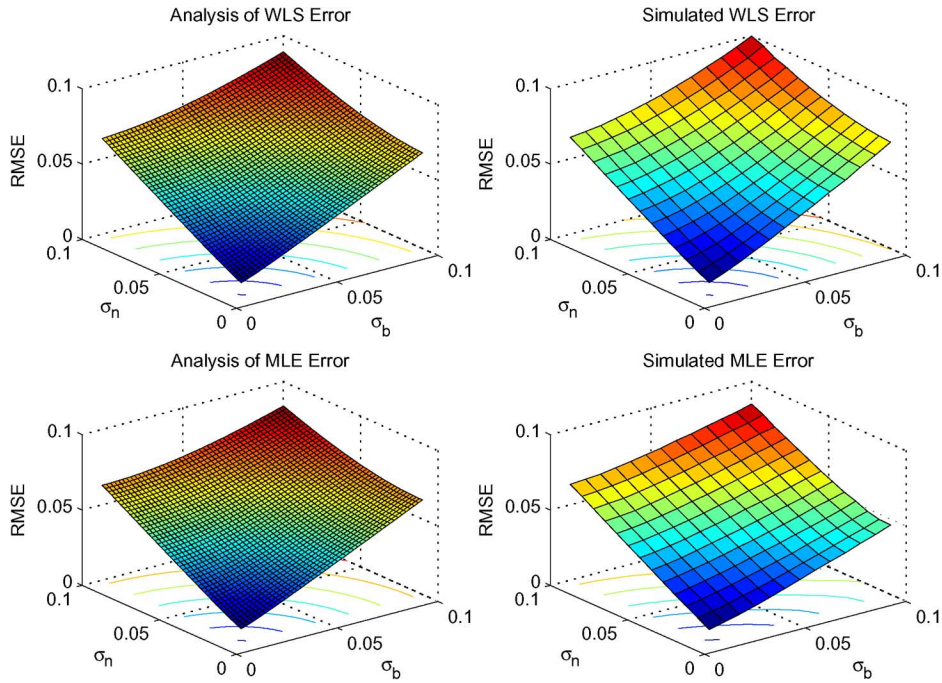

Fig. 1. Localization RMSE with a uniform circular array of 10 sensors, for WLS and MLE algorithms, as a function of additive noise standard deviation σ_n and exponential bias pdf parameter σ_b. Both algorithm simulation and analytical error prediction are shown.

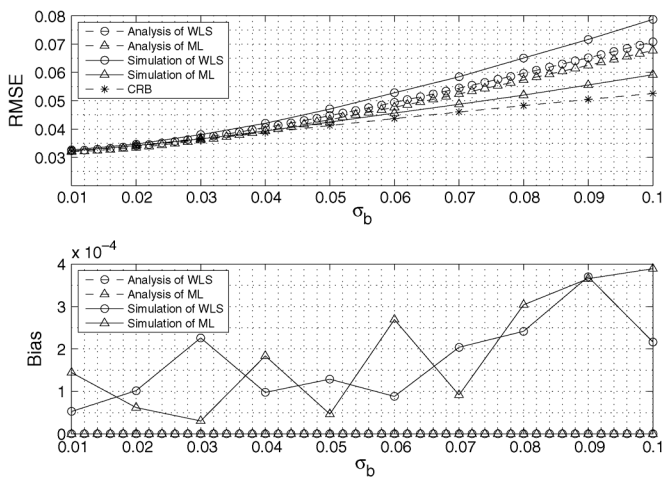

Fig. 2. RMSE and bias for geolocation, with $\sigma_n = 0.05$, using the same geometry as Fig. 1. The bias is small for this uniform circular geometry. The MLE incorporates knowledge of the bias pdf, and outperforms WLS. As $\sigma_b \to 0$, the performance is dominated by the additive noise and the RMSE converges to the CRB.

are expressed relative to the source range of 1 DU. So, for example, $\sigma_n = 0.1$ corresponds to Gaussian noise with a standard deviation of 10% of the true range (a large range error).

Fig. 1 displays the RMSE for WLS and ML estimation, comparing analysis and simulation for the two algorithms, with 10 uniformly spaced sensors on a circle. Results are depicted as a function of the exponential bias pdf parameter σ_b and the additive noise standard deviation σ_n. Fig. 2 shows RMSE and bias for the two algorithms with fixed Gaussian noise level $\sigma_n = 0.05$. The uniform circular geometry suppresses the bias in the geolocation estimate, even as σ_b increases, and bias has a very small contribution to the RMSE. The MLE has a lower RMSE than the WLS algorithm, and is closer to the CRB, which is reasonable because the MLE incorporates knowledge of the exponential bias pdf (it is a Bayesian estimate). The simulation and analysis gap grows larger for larger σ_b, as the small perturbation assumption becomes less valid, although it is a reasonable approximation. As $\sigma_b \to 0$, the RMSE for both estimators converges to the CRB. In this regime, the bias becomes negligible and the geolocation RMSE is dominated by the additive noise.

Fig. 3 continues the circular geometry example, now with $\sigma_b = 0.05$ and plotting against σ_n. As $\sigma_n \to 0$ the performance is dominated by the range bias, and so the estimators do not converge to the CRB, but instead the RMSE plateaus. The Bayesian ML algorithm continues to outperform WLS, for all noise levels. As σ_n grows, the additive noise becomes dominant and the algorithms come closer to the CRB, although with fixed $\sigma_b \neq 0$ there remains a gap between the RMSE and the CRB. As σ_n grows, there also remains a relatively small gap between the predicted and simulated errors, due to the small perturbation assumption.

In Fig. 4, we consider a case of fixed nonuniform sensor placement. The $K = 10$ sensors reside on a circle in two groups, around 0 degrees at (0, $\pm$5, $\pm$10) degrees, and around 90 degrees at (80, 85, 90, 95, 100) degrees. The WLS algorithm is dominated by the bias, which grows linearly as σ_b grows. In contrast, the MLE exploits knowledge of the exponential range bias distribution, so that the MLE location bias error remains small, and the RMSE remains close to the CRB even with σ_b rising to 0.1 (or 10% of the real distance) which is a relatively large bias. When σ_b decreases to 0.01 (or 1% of the real distance), the difference between the simulated and predicted ML results keeps shrinking although a small discrepancy remains because the error analysis accuracy is limited by the first-order perturbation technique.

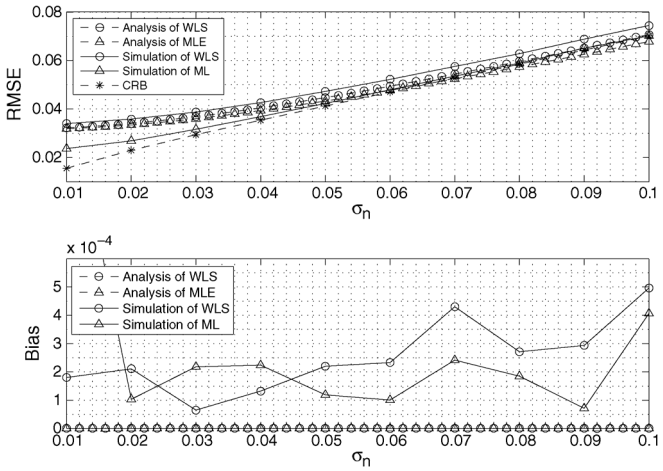

Fig. 3. Continuation of the example in Figs. 1 and 2, now fixing $\sigma_b = 0.05$. As the noise decreases ($\sigma_n \to 0$) the RMSE is dominated by the range bias, and the location error separates from the CRB.

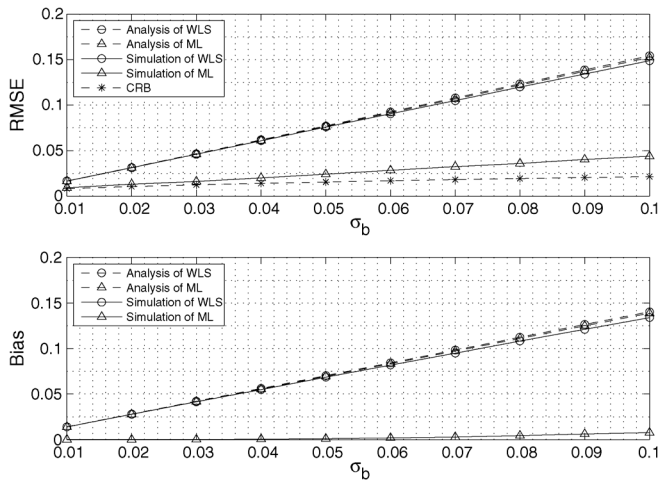

Fig. 4. Geolocation performance with $K = 10$ sensors, with two groups centered around 0 and 90 degrees (see text). The WLS algorithm geolocation error is dominated by the range bias, whereas the MLE has low bias and consequently has RMSE that remains near the CRB even for large σ_b.

Fig. 5 depicts the effect of non-i.i.d. random range measurement bias at different sensors. Here, $K = 10$ sensors are uniformly circularly spaced in order to avoid the geometry induced estimation bias. The sensors are divided into five groups with 2 sensors in each. Each two-sensor group has a common measurement bias standard deviation, with groups from 1 to 5 keeping a constant ratio of 1: 2: 4: 2: 0.5 between each other, starting from the sensor at 0 degrees and proceeding counterclockwise. All sensor measurements have the same noise standard deviation $\sigma_n = 0.01$. In Fig. 5(a), the estimation RMSE and bias are plotted versus the measurement bias standard deviation σ_b of the first group (the values for the other sensors change accordingly). It can be seen that the bias and RMSE of WLS increase at an approximate rate of twice the measurement bias σ_b. The ML estimation exploits the distribution information of the random measurement bias and greatly mitigates the estimation bias. The increasing rates of ML RMSE and bias are only 1/2 and 1/8 of σ_b, and the RMSE has a very small gap from the CRB. The scatter plot in Fig. 5(b) shows that the resulting WLS

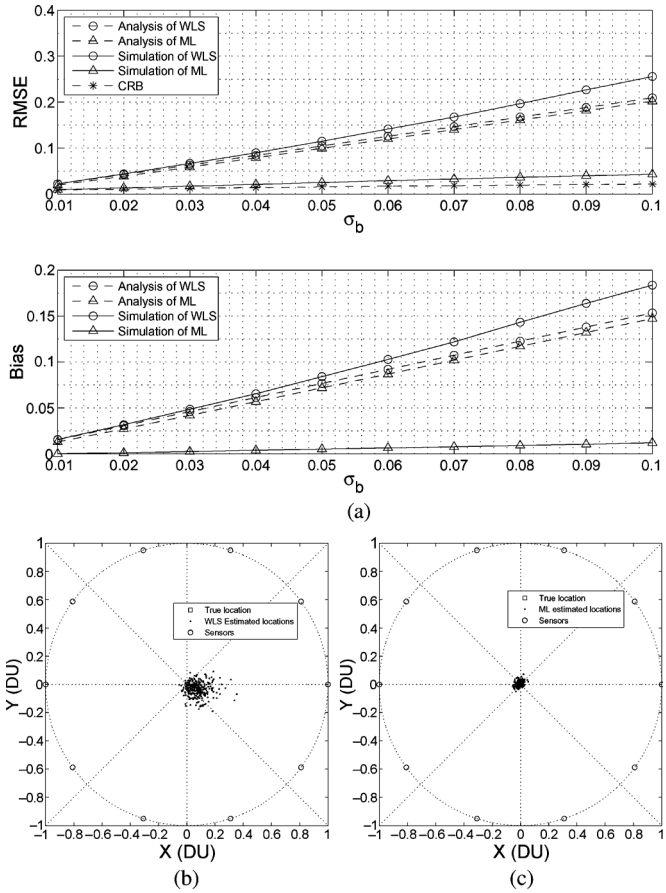

Fig. 5. Uniformly placed sensors with nonidentically distributed measurement bias (see text). This example illustrates that MLE location estimation can significantly reduce the estimation bias. (a) RMSE and bias plots. (b) Scatter plot with WLS estimation. (c) Scatter plot with ML estimation.

location estimates cluster in the fourth quadrant, which is predominantly opposite to sensor group 3 whose range measurement bias has the largest standard deviation. On the other hand, the MLE compensates for the measurement bias by exploiting the known error distributions, as reflected in Fig. 5(c).

To gain more insight into the sensor geometry effect on the estimation bias, Figs. 6 and 7 show scatter plots of WLS and ML estimation from 300 random realizations of the measurement bias and noise, respectively. Here we use $\sigma_b = 0.2$ and $\sigma_n = 0.05$ for all sensors, so that the range bias is large and the resulting geolocation bias is very evident in the scatter plots. We compare the uniform circular array and three configurations of nonuniform circular placement, with $K = 10$ sensors again confined to the circle with unity radius. In the three nonuniform cases, the sensors are split into two groups of five sensors per group. In configuration 1, both groups are placed around 0 degrees at $(\pm 1, \pm 5, \pm 10, \pm 15, \pm 20)$ degrees. Configuration 2 centers groups around 0 and 90 degrees, given by $(-10, -5,$ 0, 5, 10, 80, 85, 90, 95, 100) degrees. Configuration 3 centers around 0 and 180 degrees, at $(-10, -5,$ 0, 5, 10, 170, 175, 180, 185, 190) degrees.

The scatter plots clearly show that the estimated source location is significantly affected by the geometry of the sensor groups. The uniform array suppresses the estimation bias and both WLS and ML estimated locations appear unbiased. The

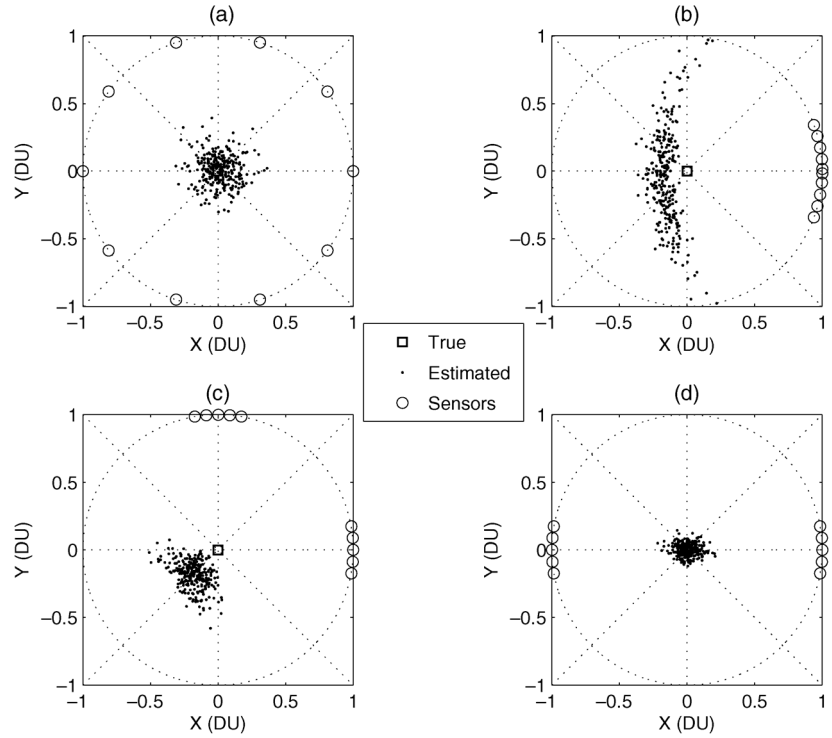

Fig. 6. Scatter plots with uniform and three nonuniform sensor placements, using WLS estimation. $\sigma_b = 0.2$, $\sigma_n = 0.05$.

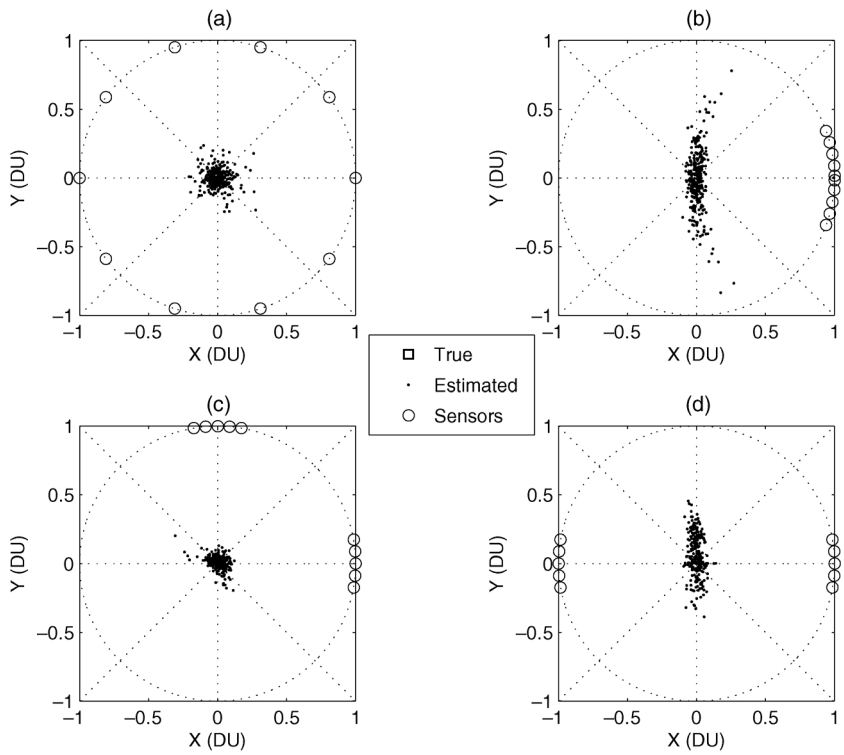

Fig. 7. Scatter plots with uniform and three nonuniform sensor placements, using ML estimation. $\sigma_b = 0.2$, $\sigma_n = 0.05$.

ML estimates tend to be more concentrated around the true location than the WLS estimates, for all configurations. However, note that in configuration 3 the WLS and MLE yield significantly different clustering shapes. From our previous examples, the MLE may generally have lower RMSE, but the 2-D bias shape depends on the geometry and the choice of algorithm.

Using the same sensor placement configurations, in Fig. 8 we show RMSE and bias plotted against σ_b, with $\sigma_n = 0.05$. As we expect, the uniform circular array has reduced sensitivity to the range bias and has the best performance of the four configurations. Configuration 3 results in the best performance among the three nonuniform sensor placement cases due to its symmetry

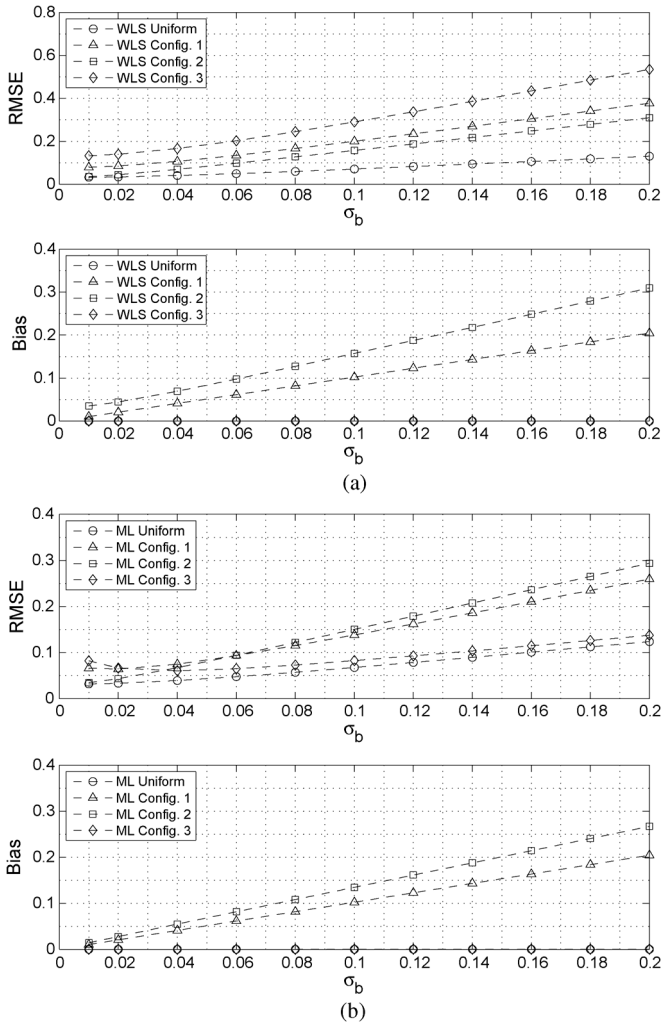

Fig. 8. Estimation RMSE and bias are plotted versus σ_b for the same configurations as in Figs. 6 and 7. (a) RMSE and bias of WLS estimation. (b) RMSE and bias of ML estimation.

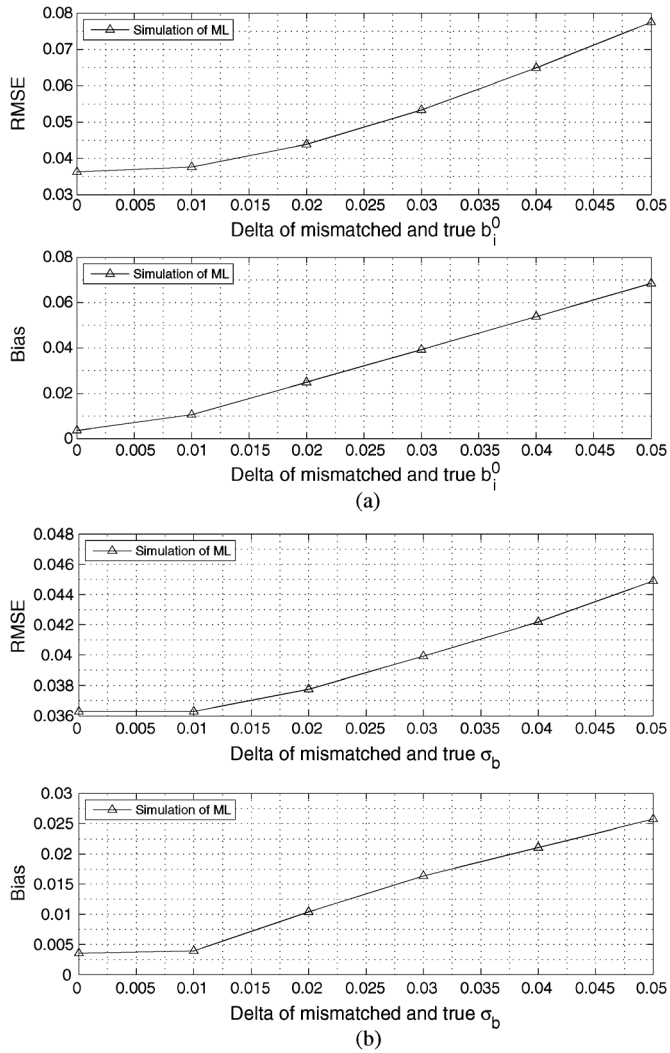

Fig. 9. The effect of mismatch in the range bias exponential distribution parameters on ML performance. The MLE is much more sensitive to mismatch in the mean of the bias distribution. (a) The case of mismatched b_i^0. (b) The case of mismatched σ_{b_i}.

around the source. The error dependence on configuration is accentuated as the range bias becomes larger.

Next we consider a case when the exponential bias pdf parameters are imperfectly known. Fig. 9 shows the effect of parameter mismatch on the localization accuracy, with the sensor configuration the same as in Fig. 4, and noise standard deviation $\sigma_n = 0.05$. In Fig. 9(a), with fixed $\sigma_{b_i} = 0.05$, the ML estimation bias and RMSE grow with an increasing gap between the actual and mismatched value of b_i^0 used in the ML estimator. The leftmost point matches the $\sigma_{b_i} = 0.05$ point in Fig. 4 with RMSE 0.036 and bias 0.0036; however, the RMSE increases to 0.077 and the bias to 0.069. In this case, the RMSE is dominated by the bias, and the estimation bias arises mostly from the mismatched statistics. In Fig. 9(b) the value of b_i^0 is fixed to 0 and the mismatched parameter is σ_{b_i}. Comparing the two, the ML estimator is much more sensitive to mismatch in the mean than in the variance, which is not surprising because the mean is added directly in the localization MLE to offset the average range bias.

As a final example, in Fig. 10 we compare geolocation estimator performance for two different range bias distributions, exponential and uniform. Fig. 10(a) is with the uniform circular array sensor geometry, and Fig. 10(b) is with a nonuniform array that has two groups of 5 sensors at 0 and 90 degrees, the same as Fig. 4. For comparison, the uniform bias is distributed in the range $[0, \beta_m]$, where β_m equals the 99% confidence point of the exponential bias. The noise standard deviation is fixed at $\sigma_n = 0.05$. The RMSE and bias for WLS and ML are plotted versus the bias standard deviation σ_b. Fig. 10(a) shows that both the WLS and ML RMSE for the uniform range bias case increases faster than for the exponential bias case. This result is reasonable, noting that our choice of β_m makes the mean of the uniform bias larger than the exponential. However, thanks to the bias cancellation effect of the uniform array, the estimation bias is similar between the two algorithms. This effect disappears in Fig. 10(b) with nonuniform sensor placement, where the WLS geolocation bias with uniform range estimation error is obviously larger than for the exponential range bias, and the geolocation RMSE is dominated by the range bias. In contrast, the ML estimator significantly suppresses the bias for both cases and the RMSE gap between the two is trivial. This is the benefit

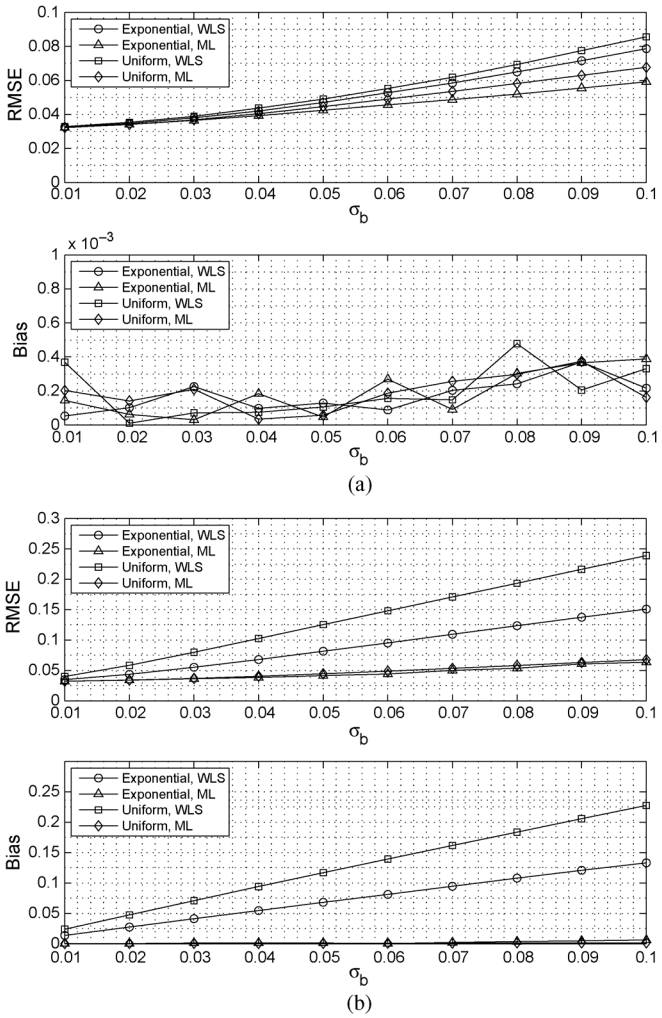

Fig. 10. A comparison of location estimation with uniformly distributed measurement bias and exponential bias. (a) The case of uniform array with 10 sensors. (b) The case of nonuniform array with two groups of 5 sensors at 0 and 90 degrees.

of exploiting the bias distribution information in the Bayesian ML estimation.

VII. Conclusion

We have investigated the performance of geolocation based on range measurements, when the measured range may have a positive bias arising from nonline of sight propagation. We considered deterministic and random models for the range bias, and analyzed both weighted least squares and maximum likelihood geolocation estimators. The analysis enables combined study of the effects of the sensor geometry and the range estimate quality on the resulting geolocation estimates, which we examined through both RMSE and bias error terms for the WLS and MLE algorithms. The small error perturbation analysis provided good approximations for algorithm performance with relatively simple expressions, as a function of the key system parameters.

Biased range measurements generally result in biased geolocation estimates, although spatial diversity in sensor placement results in lower bias. We considered analysis and simulation of several sensor configurations to demonstrate this. When the range bias becomes small, the resulting geolocation estimates are noise-dominated, and approach the CRB as the noise variance decreases. While the CRB is a bound only on unbiased estimates, it provides a useful benchmark in our examples.

The MLE algorithm with a random model on the range measurement is a Bayesian estimator, incorporating knowledge of the range bias distribution. Consequently, the MLE is much more robust to the range measurement bias, although its use in practice may require characterizing the propagation environment. The WLS approach provides a general framework for algorithms, and prior knowledge can be incorporated via the weights (which is also a topic for further work).

Appendix I

Measurement Error Distribution With Maxwell and Uniform Range Bias Models

We derive the measurement error distributions for the cases of Maxwell and uniform random range bias models, with additive white Gaussian noise. These may be used to find the location MLE and its small error performance, as we did for the exponential random bias model in Section IV.

A. Maxwell Range Measurement Bias Distribution

Here, the bias distribution follows (7), where the bias b_i has standard deviation σ_{b_i} and mean $\mu_{b_i} = \frac{2\sqrt{2}}{\sqrt{3\pi-8}}\sigma_{b_i}$. So, the distribution of v_i is

$$\begin{aligned} f_{v_i}(v_i) &= \int_0^\infty h_{b_i}(x) g_{n_i}(v_i - x)dx \\ &= \frac{(3-8/\pi)^{3/2}}{\pi\sigma_{b_i}^3\sigma_n} \\ &\quad \times \int_0^\infty x^2 \exp\left[-\frac{(3-8/\pi)x^2}{2\sigma_{b_i}^2} - \frac{(v_i-x)^2}{2\sigma_n^2}\right]dx \end{aligned} \quad (81)$$

which does not have a closed-form expression.

B. Uniform Range Measurement Bias Distribution

Here, the bias b_i follows a uniform distribution (6), with standard deviation σ_{b_i} and mean $\mu_{b_i} = \frac{\beta_{s,i}+\beta_{m,i}}{2}$. The resulting distribution of v_i is

$$\begin{aligned} f_{v_i}(v_i) &= \int_{\beta_{s,i}}^{\beta_{m,i}} h_{b_i}(x) g_{n_i}(v_i - x)dx \\ &= \frac{1}{\beta_{m,i}-\beta_{s,i}} \int_{\beta_{s,i}}^{\beta_{m,i}} \frac{1}{\sqrt{2\pi}\sigma_n} \exp\left[-\frac{(v_i-x)^2}{2\sigma_n^2}\right]dx \\ &= \frac{1}{\beta_{m,i}-\beta_{s,i}}\left[Q\left(\frac{v_i-\beta_{m,i}}{\sigma_n}\right) - Q\left(\frac{v_i-\beta_{s,i}}{\sigma_n}\right)\right]. \end{aligned} \quad (82)$$

To obtain the MLE for this model, the derivative of $f_{v_i}(v_i)$ is found as

$$f'_{v_i}(v_i) = -\frac{1}{\beta_{m,i}-\beta_{s,i}}\left[e^{-\frac{(v_i-\beta_{m,i})^2}{2\sigma_n^2}} - e^{-\frac{(v_i-\beta_{s,i})^2}{2\sigma_n^2}}\right].$$

Substituting $f_{v_i}(v_i)$ and $f'_{v_i}(v_i)$ into (37) and (38), we find the MLE constraint equations to be

$$\frac{1}{\sqrt{2\pi}\sigma_n}\sum_{i=1}^{K}\frac{e^{-\frac{(r_i-d_i-\beta_{m,i})^2}{2\sigma_n^2}}-e^{-\frac{(r_i-d_i-\beta_{s,i})^2}{2\sigma_n^2}}}{Q\left(\frac{r_i-d_i-\beta_{m,i}}{\sigma_n}\right)-Q\left(\frac{r_i-d_i-\beta_{s,i}}{\sigma_n}\right)}\cos\theta_i=0 \quad (83)$$

$$\frac{1}{\sqrt{2\pi}\sigma_n}\sum_{i=1}^{K}\frac{e^{-\frac{(r_i-d_i-\beta_{m,i})^2}{2\sigma_n^2}}-e^{-\frac{(r_i-d_i-\beta_{s,i})^2}{2\sigma_n^2}}}{Q\left(\frac{r_i-d_i-\beta_{m,i}}{\sigma_n}\right)-Q\left(\frac{r_i-d_i-\beta_{s,i}}{\sigma_n}\right)}\sin\theta_i=0. \quad (84)$$

APPENDIX I

RELATING THE DETERMINISTIC AND RANDOM MODELS

In this appendix we show the connection between the deterministic and random cases for range bias, including the perturbation error analysis. We can recover the deterministic model results from the random bias measurement model case as follows. We focus on the exponential measurement bias model case from Section IV-B, although the ideas are general. Letting all $\sigma_{b_i}\to 0$ in the exponential pdf (5) causes both the mean and the standard deviation to diminish. The random bias b_i reverts to the deterministic known value b_i^0. In this case, the exponential pdf reduces to a delta function and the pdf of the measurement error reduces to a Gaussian form. Using the definition of the Q-function, noting that $Q(\infty)=0$ and applying L'Hopital's rule, we can show that the pdf of v_i can be obtained from (40) by taking the limit

$$\lim_{\sigma_{b_i}\to 0} f_i(v_i)=\lim_{\sigma_{b_i}\to 0}\frac{Q\left(\frac{b_i^0-v_i+\sigma_{n_i}^2/\sigma_{b_i}}{\sigma_{n_i}}\right)}{\sigma_{b_i}\exp\left(\frac{v_i-b_i^0}{\sigma_{b_i}}-\frac{\sigma_{n_i}^2}{2\sigma_{b_i}^2}\right)}=g_i\left(v_i-b_i^0\right). \quad (85)$$

Thus in the limiting case, $f_i(v_i)$ takes a Gaussian pdf form with mean b_i^0 and variance $\sigma_{n_i}^2$.

From this, we should expect the error analysis result for the ML estimation in this limiting case to be the same as the WLS result (19) with $w_i=\frac{1}{\sigma_i^2}$. Differentiating (85) we have

$$\lim_{\sigma_{b_i}\to 0} f_i'(v_i)=-\frac{v-b_i^0}{\sigma_{n_i}^2}g_i\left(v-b_i^0\right)=-\frac{v-b_i^0}{\sigma_{n_i}^2}\lim_{\sigma_{b_i}\to 0} f_i(v_i). \quad (86)$$

Substituting (86) into (37) and (38), the ML estimate satisfies

$$\sum_{i=1}^{K}\frac{1}{\sigma_{n_i}^2}\left[\left(r_i-b_i^0\right)-d_i\right]\cos\theta_i=0 \quad (87)$$

$$\sum_{i=1}^{K}\frac{1}{\sigma_{n_i}^2}\left[\left(r_i-b_i^0\right)-d_i\right]\sin\theta_i=0 \quad (88)$$

which have the same form as the WLS (9) and (10) with $w_i=\frac{1}{\sigma_i^2}$, except that the deterministic known bias b_i^0 is subtracted from the measurement r_i. In the error analysis, because $\delta(r_i-b_i^0)=\delta(r_i)$, and replacing $r_i-b_i^0$ with d_i, we obtain the same expression as (19). Therefore, the performance of the ML estimator for this limiting case and the WLS estimator for the deterministic bias case are equivalent.

We establish the consistency in the perturbation error analyses for the two cases as follows. We note that the bias and MSE expressions (20), (22) and (66), (65) are similar. With all $\sigma_{b_i}\to 0$, the random bias mean μ_{b_i} becomes a deterministic bias b_i, and the error correlation matrix $\mathbf{\Psi}$ becomes $\mathbf{\Phi}_v$. Thus, to prove the equivalence between WLS and ML in the limiting case, it suffices to show

$$\lim_{\forall\sigma_{b_i}\to 0}\mathbf{U}=\mathbf{C},\quad \lim_{\forall\sigma_{b_i}\to 0}\mathbf{T}=\mathbf{D}. \quad (89)$$

Note that the elements of matrices $\mathbf{U}$ and $\mathbf{T}$ depend on $f_i(b_i^0)$ given by (41). To proceed we can employ the large x expansion of the Q-function, given by [21]

$$Q(x)=\frac{e^{-\frac{x^2}{2}}}{x\sqrt{2\pi}}\sum_{k=0}^{\infty}\frac{(-1)^k(2k)!}{k!(\sqrt{2}x)^{2k}},\quad \text{for large } x. \quad (90)$$

So, (41) becomes

$$f_i\left(b_i^0\right)=\frac{1}{\sqrt{2\pi}\sigma_{n_i}}\sum_{k=0}^{\infty}\frac{(-1)^k(2k)!\sigma_{b_i}^{2k}}{k!\left(\sqrt{2}\sigma_{n_i}\right)^{2k}} \quad (91)$$

from which we obtain

$$\lim_{\sigma_{b_i}\to 0} f_i\left(b_i^0\right)=\frac{1}{\sqrt{2\pi}\sigma_{n_i}}=g_i(0) \quad (92)$$

which corresponds to the result in (85). We can continue and find

$$\lim_{\sigma_{b_i}\to 0}\frac{g_i(0)-f_i\left(b_i^0\right)}{\sigma_{b_i}^2}=\frac{1}{\sqrt{2\pi}\sigma_{n_i}^3}=\frac{g_i(0)}{\sigma_{n_i}^2}. \quad (93)$$

With the above, we will find the limiting results for elements of $\mathbf{U}$. We discard the second term in (58) since it is negligible compared to the first term that contains the factor $\frac{1}{\sigma_{b_i}}$. Applying (93) and (92) successively to that equation, we obtain

$$\begin{aligned}\lim_{\sigma_{b_i}\to 0} u_{11}&=\lim_{\sigma_{b_i}\to 0}\sum_{i=1}^{K}\frac{\cos^2\theta_i g_i(0)\left[g_i(0)-f_i\left(b_i^0\right)\right]}{\sigma_{b_i}^2 f_i^2\left(b_i^0\right)}\\&=\lim_{\sigma_{b_i}\to 0}\sum_{i=1}^{K}\frac{\cos^2\theta_i g_i^2(0)}{\sigma_{n_i}^2 f_i^2\left(b_i^0\right)}\\&=\sum_{i=1}^{K}\frac{\cos^2\theta_i}{\sigma_{n_i}^2}\end{aligned} \quad (94)$$

which is the same as c_{11} in (18) with $w_i=\frac{1}{\sigma_{n_i}^2}$. Similarly we can establish convergence of the other elements of $\mathbf{U}$ to those of $\mathbf{C}$, and $\mathbf{T}$ to $\mathbf{D}$. Therefore, (89) follows, and the two cases are equivalent. This equivalence proof validates our derivation in Section IV-B-3.

ACKNOWLEDGMENT

The authors gratefully acknowledge the contribution of Prof. R. Kozick.

REFERENCES

[1] B. M. Sadler, N. Liu, Z. Xu, and R. Kozick, "Range-based geolocation in fading environments," in *Proc. 46th Ann. Allerton Conf. Commun., Contr., Comput.*, Urbana-Champaign, IL, Sep. 2008, pp. 15–20.

[2] N. Patwari, J. N. Ash, S. Kyperountas, A. O. Hero, R. L. Moses, and N. S. Correal, "Locating the nodes: Cooperative localization in wireless sensor networks," *IEEE Signal Process. Mag.*, vol. 22, no. 4, pp. 54–69, Jul. 2005.
[3] S. Pandey and P. Agrawal, "A survey on localization techniques for wireless networks," *J. Chinese Inst. of Eng.*, vol. 29, no. 7, pp. 1125–1148, 2006.
[4] D. Niculescu, "Positioning in ad hoc sensor networks," *IEEE Network*, vol. 18, no. 4, pp. 24–29, Jul./Aug. 2004.
[5] J. F. Bull, "Wireless geolocation," *IEEE Veh. Technol. Mag.*, vol. 4, no. 4, pp. 45–53, Dec. 2009.
[6] R. L. Moses, D. Krishnamurthy, and R. Patterson, "A self-localization method for wireless sensor networks," *EURASIP J. Appl. Signal Process.*, vol. 2003, no. 4, pp. 348–358, Mar. 2003.
[7] N. Patwari, A. O. Hero, M. Perkins, N. S. Correal, and R. J. O'Dea, "Relative location estimation in wireless sensor networks," *IEEE Trans. Signal Process.*, vol. 51, no. 8, pp. 2137–2148, Aug. 2003.
[8] A. Savvides, W. L. Garber, R. L. Moses, and M. B. Srivastava, "An analysis of error inducing parameters in multihop sensor node localization," *IEEE Trans. Mobile Comput.*, vol. 4, no. 6, pp. 567–577, Nov./Dec. 2005.
[9] B. M. Sadler, R. J. Kozick, and L. Tong, "Multi-modal sensor localization using a mobile access point," in *Proc. IEEE Intl. Conf. Acoust., Speech, Signal Process.*, 2005.
[10] W. C. Y. Lee, *Mobile Communications Engineering: Theory and Applications*, 2nd ed. New York: McGraw-Hill, 1998.
[11] W. C. Jakes, *Microwave Mobile Communications*. New York: Wiley, 1974.
[12] J. D. Parsons, *The Mobile Radio Propagation Channel*, 2nd ed. New York: Wiley, 2000.
[13] *An Introduction to Ultra Wideband Communication Systems*, J. H. Reed, Ed. Englewood Cliffs, NJ: Prentice-Hall, 2005.
[14] *Ultra-Wideband Antennas and Propagation for Communications, Radar and Imaging*, B. Allen, M. Dohler, E. E. Okon, W. Q. Malik, A. K. Brown, and D. J. Edwards, Eds. New York: Wiley, 2007.
[15] N. A. Alsindi, B. Alavi, and K. Pahlavan, "Measurement and modeling of ultrawideband TOA-based ranging in indoor multipath environments," *IEEE Trans. Veh. Technol.*, vol. 58, no. 3, pp. 1046–1058, Mar. 2009.
[16] A. J. Weiss and J. S. Picard, "Network localization with biased range measurements," *IEEE Trans. Wireless Commun.*, vol. 7, no. 1, pp. 298–304, Jan. 2008.
[17] D. B. Jourdan, D. Dardari, and M. Z. Win, "Position error bound for UWB localization in dense cluttered environments," *IEEE Trans. Aerosp. Electron. Syst.*, vol. 44, no. 2, pp. 613–628, Apr. 2008.
[18] Y. Qi, H. Kobayashi, and H. Suda, "On time-of-arrival positioning in a multipath environment," *IEEE Trans. Vech. Technol.*, vol. 55, no. 5, pp. 1516–1526, Sep. 2006.
[19] N. Liu, Z. Xu, and B. M. Sadler, "Low-complexity hyperbolic source localization with a linear sensor array," *IEEE Signal Process. Lett.*, vol. 15, pp. 865–868, November 2008.
[20] A. Swami, "Cramer-Rao bounds for deterministic signals in additive and multiplicative noise," *Signal Process.*, vol. 53, no. 2, pp. 231–244, Sep. 1996.
[21] Z. Xu and B. M. Sadler, "Time delay estimation bounds in convolutive random channels," *IEEE J. Sel. Topics Signal Process.*, vol. 1, no. 3, pp. 418–430, Oct. 2007.

Ning Liu received the B.E. and M.E. degrees in communication engineering from Xidian University, Xi'an, China, in 2000 and 2003, respectively, and the Ph.D. degree in electrical engineering from University of California, Riverside, in 2010.

From 2003 to 2006, he was a system engineer in Datang Mobile Communications Equipment Company, Beijing, China. He is currently an engineer in Broadcom Corporation, Irvine, CA. His research interests include statistical signal processing, transceiver design for wireless communication systems, cooperative localization and tracking for cellular and wireless sensor networks, and time delay estimation.

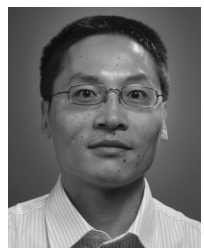

Zhengyuan Xu (S'97–M'99–SM'02) received the B.S. and M.S. degrees in electronic engineering from Tsinghua University, Beijing, China, in 1989 and 1991, respectively, and the Ph.D. degree in electrical engineering from Stevens Institute of Technology, Hoboken, NJ, in 1999.

From 1991 to 1996, he was a System Engineer and Department Manager at the Tsinghua Unisplendour Group Corporation, Tsinghua University. In 1999, he joined the Department of Electrical Engineering, University of California at Riverside, as an Assistant Professor, and was promoted to Associate Professor with tenure and Professor later on. He was Founding Director of the Multi-campus Center for Ubiquitous Communication by Light (UC-Light), University of California. In 2010, he was selected by the "Thousand Talents Program" of China, and appointed as a National Distinguished Professor in the Department of Electronic Engineering and Tsinghua National Laboratory of Information Science and Technology, Tsinghua University. His Optical Wireless Information Systems (OWisys) Laboratory focuses on research in wireless communications, networking, optical wireless communication, geolocation, intelligent transportation systems, and signal processing. He has published over 150 journal and conference papers.

Dr. Xu has served as an Associate Editor and Guest Editor for various IEEE journals in communications, vehicle technology, or signal processing. He has served as a Chair, Session Chair, Technical Program Committee Chair and member for numerous international conferences. He was also an elected member of the IEEE Signal Processing Society's Technical Committee on Signal Processing for Communications for six years.

Brian M. Sadler (S'81–M'81–SM'02–F'07) received the B.S. and M.S. degrees from the University of Maryland, College Park, and the Ph.D. degree from the University of Virginia, Charlottesville, all in electrical engineering.

He is a Fellow of the Army Research Laboratory (ARL) in Adelphi, MD. His research interests include information science, networked and autonomous systems, sensing, and mixed-signal integrated circuit architectures.

Dr. Sadler is an Associate Editor for EURASIP *Signal Processing*, was an Associate Editor for the IEEE TRANSACTIONS ON SIGNAL PROCESSING and IEEE SIGNAL PROCESSING LETTERS, and has been a Guest Editor for several journals including the IEEE JOURNAL ON SELECTED TOPICS IN SIGNAL PROCESSING, IEEE JOURNAL ON SELECTED AREAS IN COMMUNICATION, and the IEEE SIGNAL PROCESSING MAGAZINE. He is a member of the IEEE Signal Processing Society Sensor Array and Multi-channel Technical Committee. He received Best Paper Awards from the Signal Processing Society in 2006 and 2010. He has received several ARL and Army R&D awards, as well as a 2008 Outstanding Invention of the Year Award from the University of Maryland.